Supporting Information for:

Decomposition of Fluoroethylene Carbonate Additive and Glue Effect of Lithium Fluoride Products for Solid Electrolyte Interphase: An Ab-Initio Study

Yukihiro Okuno[a,b,*],Keisuke Ushirogata[a,b], Keitaro Sodeyama[b,c], and Yoshitaka Tateyama[b,d,*]

a. Research and Development Management Headquarters, FUJIFILM Corporation, 210 Nakanuma, Minamiashigara, Kanagawa 250-0193, Japan

b. International Center for Materials Nanoarchitectonics (MANA), National Institute for Materials Science (NIMS), 1-1 Namiki, Tsukuba, Ibaraki 305-0044, Japan

c. PRESTO, Japan Science and Technology Agency (JST), 4-1-8 Honcho, Kawaguchi, Saitama 333-0012, Japan

d. Elements Strategy Initiative for Catalysts & Batteries, Kyoto University, Goryo-Ohara, Nishikyo-ku, Kyoto 615-8245, Japan,

* E-mail yukihiro.okuno@fujifilm.com
* E-mail TATEYAMA.Yoshitaka@nims.go.jp

1. Results of Cluster Boundary Condition Density Functional Theory

In this section of Electric Supporting Information (ESI), we show the results of CBC-DFT calculation. We used B3LYP functional with basis set aug-cc-pVTZ and PCM technique with dielectric constant $\varepsilon = 89.78$. First, we show the atomic charges of FEC estimated with the Natural Population Analysis in the DFT cluster calculations of FEC and Li^+-FEC molecules in the EC solvent.

Table S1 Natural population analysis of neutral FEC and FEC anion.

	O_1	O_F	Oc	C_H	C_F	Cc	F
Neutral	-0.603	-0.510	-0.496	0.987	0.467	-0.099	-0.372
Anion	-0.809	-0.637	-0.615	0.634	0.461	-0.102	-0.448

From the natural population analysis, we can see the excess electron in anion radical FEC is localized in CO_3 moiety of molecule.

Next, we show the energy diagram of ring cleavage of anion radical FEC for SF, WF, and WC bonds cleavage, where SF=C_C-O_F, WC=C_C-O_H, and WF=C_F-O_F bonds of FEC.

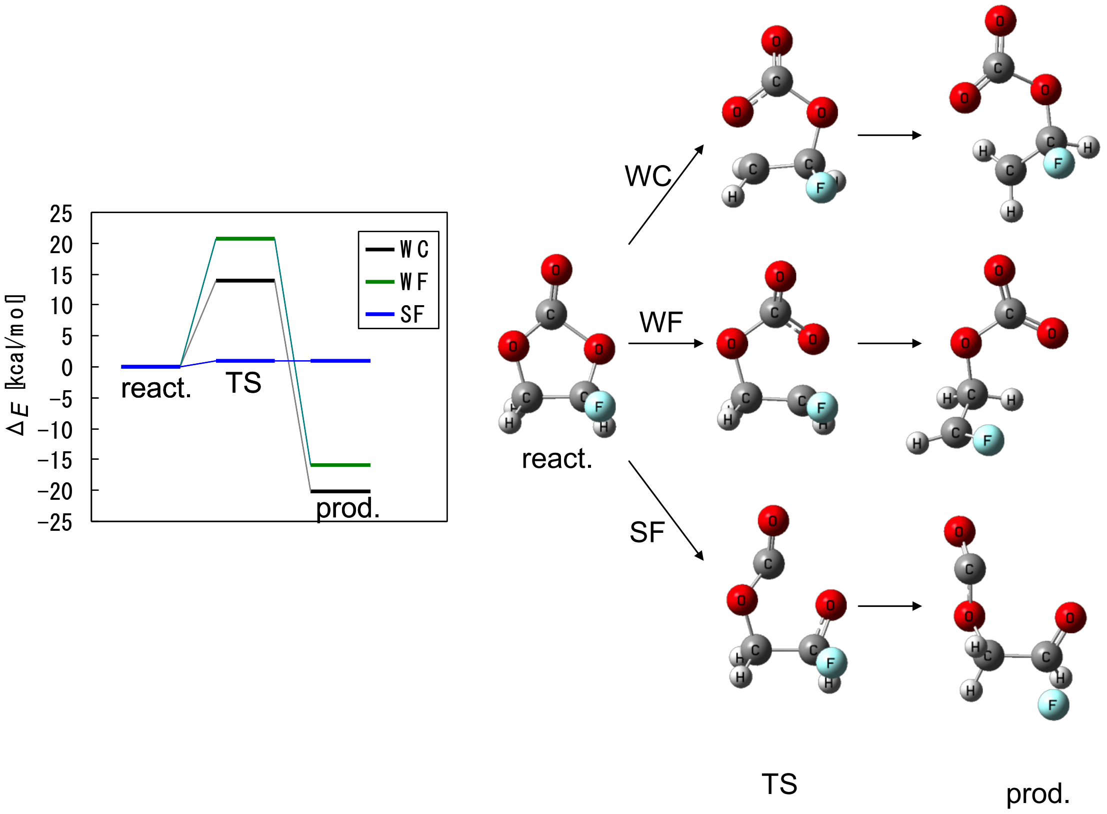

Figure S1 Energy diagram of ring cleavage of anion radical FEC^-, where TS is the transition state of the bond cleavage reaction.

From Fig.S1, we can see the “waist “ bonds of FEC (WC and WF) have large reaction energies, however, their activation energies are also large. On the other hand, the activation energy of SF bond is very small. These results are consistent to our DFT-MD results with blue-moon ensemble technique.

To examine the electron transfer that has frequently occurred in DFT-MD calculation in the cases of WC/WF bond breaking of FEC$^-$, we show the comparison of energies among the states of EC + FEC with 1 excess electron.

Table S2 Energies of EC + FEC with 1 excess electron.

	EC + FEC$^-$	EC + FEC$^-$(WC-TS)	EC + FEC$^-$(WF-TS)	EC$^-$ + FEC	*EC$^-$ + FEC
ΔE[kcal/mol]	0.0	14.0	20.6	7.9	20.2

*EC$^-$: The anion radical EC with the closed ring structure of neutral EC.

From the comparison of energies in Table S2, we can see that the electron transfer from FEC$^-$ to neutral EC can easily occur in WC (WF) bond cleavage transition state (TS) of FEC$^-$.

The wave function analysis of SF-bond breaking anion-radical FEC$^-$ is shown in Figure S2.

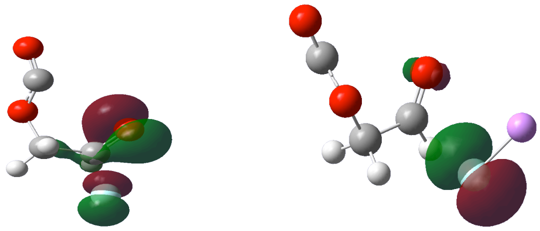

HOMO-2 HOMO-2

Figure S2 Wave function structure of HOMO-2 in SF bond breaking FEC$^-$ (left) and FEC reacted with Li (right).

We can see that the HOMO-2 of SF-bond cleavage FEC$^-$ has some σ * characteristic in C_F-F bond originated from the orbital hybridization of F’s p_σ orbital. This HOMO-2 orbital induces the bond cleavage of C_F-F bond. Actually, we located Li$^+$ ion near the F atom in FEC and optimized the structure of FEC + Li , we got the structure of FEC with bond breaking of C_F-F.

2. Results of Density Functional Theory Based Molecular Dynamics

In this section, we show the supporting information on the results of DFT-MD calculation.

In Figure S.3, we show the representative snapshots of Li-4EC and Li-3EC1FEC solvation structures obtained in the DFT-MD runs.

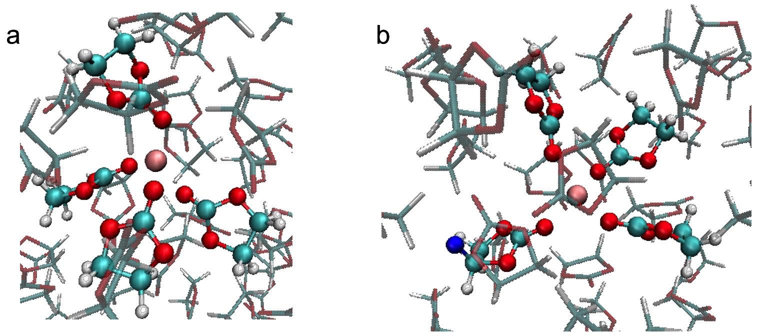

Figure S3 Snapshots in the DFT-MD trajectories of (a) Li-4EC and (b) Li-3EC1FEC systems.

Next, we show the free energy profile of the reaction between neutral FEC and neutral radical d_F-FEC in Figure S4. We set the mechanical constraints ξ of the distance between target C_F of FEC and $C_C^{\cdot}$ of d_F-FEC and carried out DFT-MD run with blue-moon ensemble techniques. The result shows the reaction is endothermic and neutral radical d_F-FEC is inert to neutral FEC.

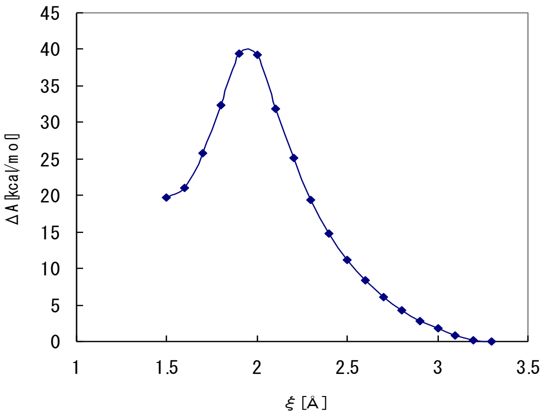

Figure S4 Free Energy profile of binding reaction between neutral FEC and neutral radical d_F-FEC along the mechanical constraint ξ of the distance between C_F of FEC and $C_C^{\cdot}$ of d_F-FEC.

Then, we show the density of state (DOS) in equilibrium state of 40 Li_2EDC with 10 LiF molecules mixture in Figure S5.

In Figure S.5, we can see that Li (F) partial density of state (PDOS) is located well above (below) the conduction (valence) band bottom (top). Therefore, the insulating properties of the Li_2EDC aggregates are not affected by the mixture of LiF molecules in the SEI film.

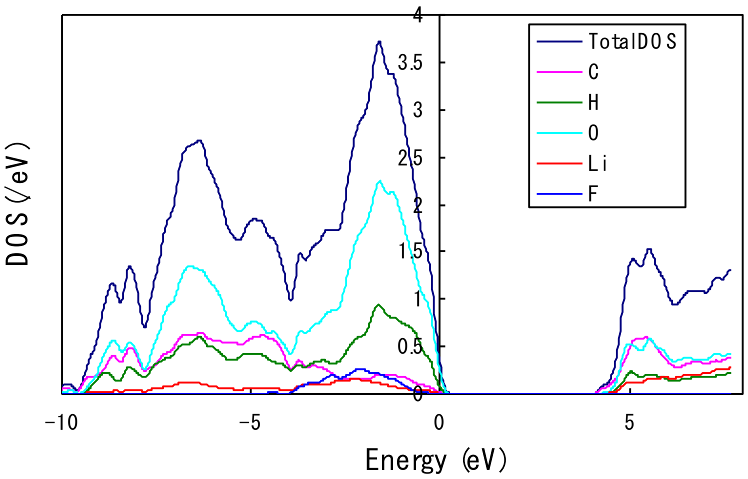

Figure S5 Partial DOS of equilibrium state of 10 LiF mixture in 40 Li_2EDC.

Figure S6 shows the radical distribution function from F atom to Li atom in 40 Li_2EDC with 10 LIF. F atom is surrounded by Li atom at the F-Li distance of about 1.86 Å.

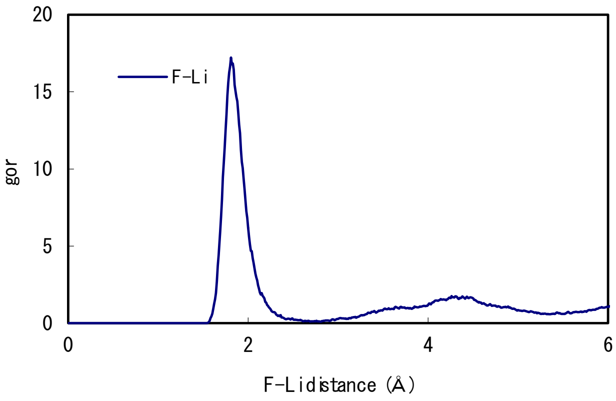

Figure S6 Radical Distribution function from F atom to Li atom in 40 Li_2EDC with 10 LiF.

We show the representative snap shots of DFT-MD trajectory of equilibrium state of LiF/ Li_2EDC interface in EC electrolyte (Figure S7) and their energy trajectories (Figure S8). The calculated box is 16.4292x38.3623x16.4292 (16.4292x50.7504x16.4292) (Å) for 67 (72) EC molecules with one Li_2EDC molecule (16 Li_2EDC aggregate) case, and we set LiF layer by 128 LiF amorphous state.

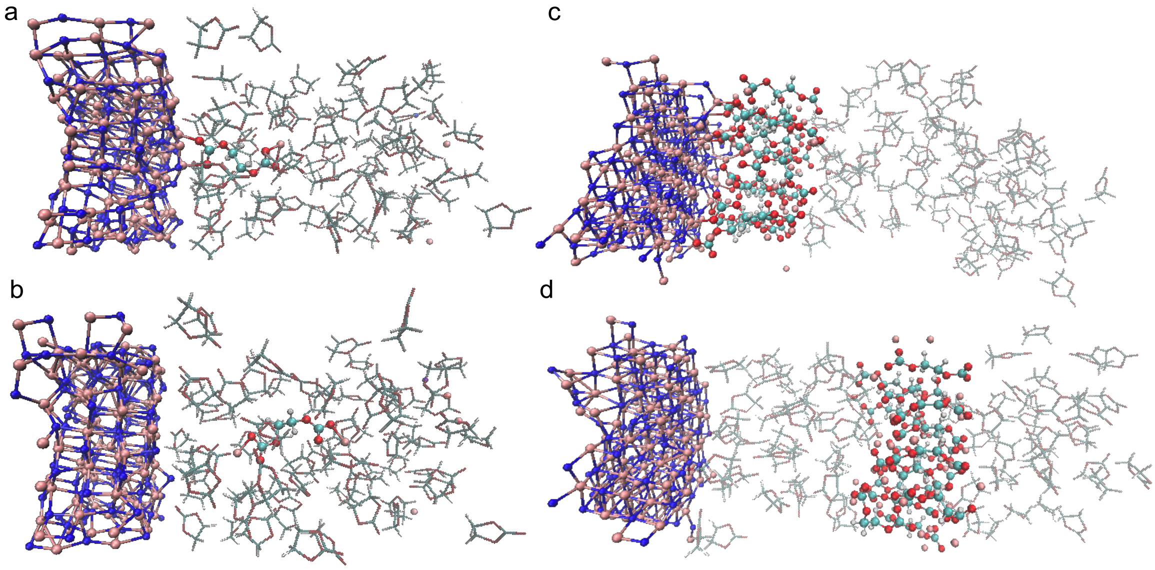

Figure S7. DFT-MD snapshots of LiF/ Li_2EDC interface in EC electrolyte. LiF and Li_2EDC are shown in the ball and stick style, while the diaphanous tube style is used for EC solvent molecules. Cyan, white, red, blue and pink colors denote C, H, O, F and Li atoms, respectively. (a,b) and (c,d) show 128 LiF + one Li_2EDC + 67 EC and 128 LiF + 16 Li_2EDC + 72 EC, respectively.

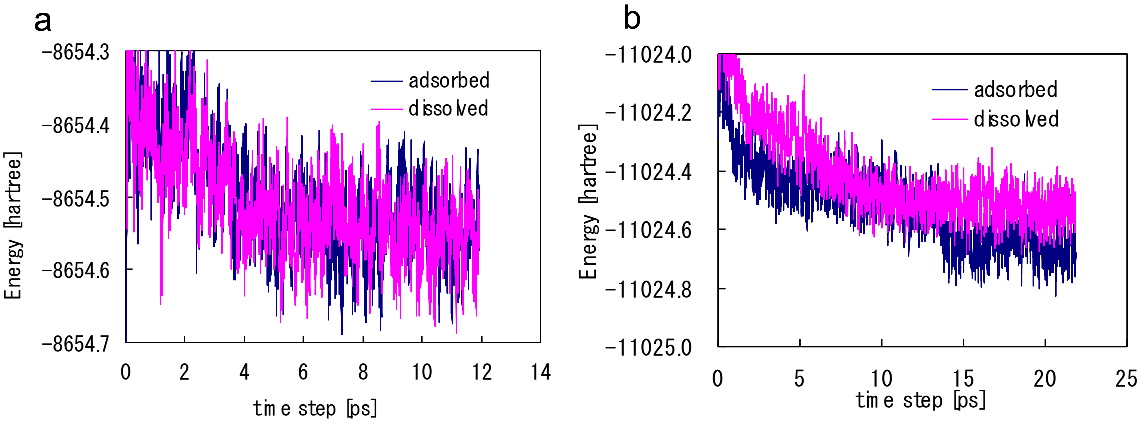

Figure S8. Energy trajectories in the DFT-MD calculations for Li_2EDC adsorbed and dissolved states, (a) 128 LiF + one Li_2EDC + 67 EC, (b) 128 LiF + 16 Li_2EDC + 72 EC.

In order to examine the adhesion properties of LiF aggregate to graphite and lithiated silicon electrodes, we performed DFT-MD calculation of adsorbed and dissolved state of LiF aggregate and calculated the adsorption energies of LiF aggregate to the electrodes in EC electrolyte.

For the H-caped graphite electrode case, the electrode consists of four graphite sheets, where each sheet has 5 × 6 hexagonal rings modeled as $C_{288}H_{46}Li_{12}$. LiF aggregate consists of 64 LiF and EC electrolyte is 60 EC molecules. The size of calculated box is 14.9130 x 48.8110 x 14.8240 (Å).

For the case of lithiated silicon electrode case, the electrode is modeled by LiSi alloy of $Li_{64}Si_{64}$ slab structure. LiF aggregate and EC electrolyte consist of 64 LiF and 64 EC molecules, respectively.

The size of calculated box is 13.2271 x 61.5615 x 13.2271 (Å).

Figure S9 shows the DFT-MD snapshots of LiF aggregate adhesion and dissolution structures in the graphite electrode case.

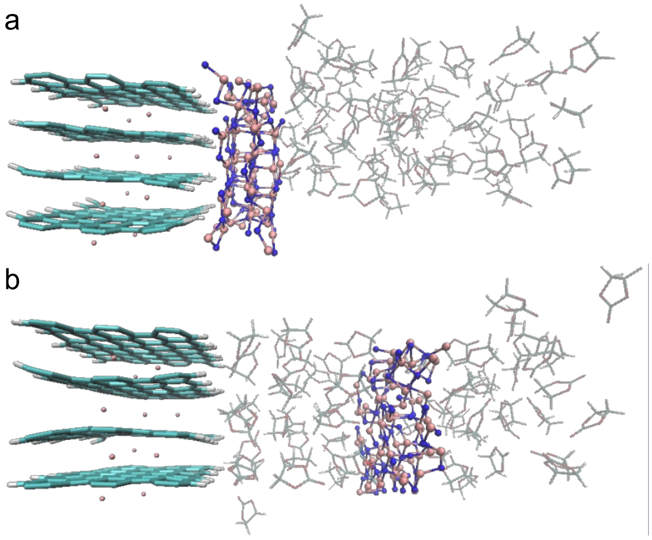

Figure S9. DFT-MD snapshots of graphite electrode / EC electrolyte interface with LiF. Graphite and intercalated Li are displayed in the tube style. The SFCs are shown in the ball and stick style, while the diaphanous tube style is used for EC solvent molecules. Cyan, white, red, blue and pink colors denote C, H, O, F and Li atoms, respectively. (a) Adsorbed structure of LiF aggregate to graphite anode. (b) Dissolved structure of LiF aggregate in EC electrolyte.

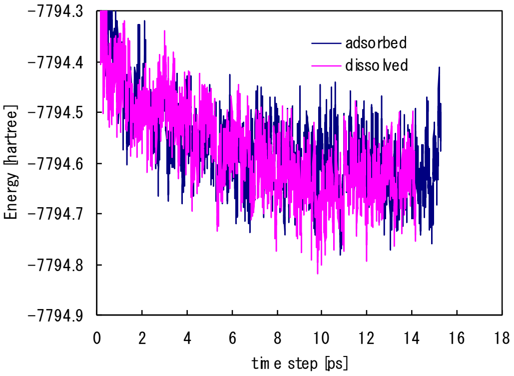

Figure S10. Energy trajectories in the DFT-MD calculations for the adsorbed and dissolved structure of LiF aggregate in graphite electrode case.

The average energy of LiF adsorbed state to the graphite electrode is 18.7 kcal/mol higher than that of LiF dissolved state. On the other hand in the lithiated silicon case, we observed the reductive decomposition of EC molecules near the surface of lithiated silicon. The EC molecules are directly contacted to lithiated silicon anode even in LiF adsorbed state due to the periodic boundary condition of calculated supercell. The numbers of decomposed EC molecules in adsorbed and dissolved cases are different. (2 EC and 3 EC molecules are decomposed in adsorbed and dissolved structure cases, respectively.) Therefore, we cannot estimate the adsorption energy of LiF aggregate to lithiated silicon by subtraction of the total energies of adsorbed and dissolved structures._ Interestingly, there is no decomposition of EC near the LiF aggregate adsorbed surface. This result indicates that LiF aggregate is insulating enough against EC solvent for silicon anode.

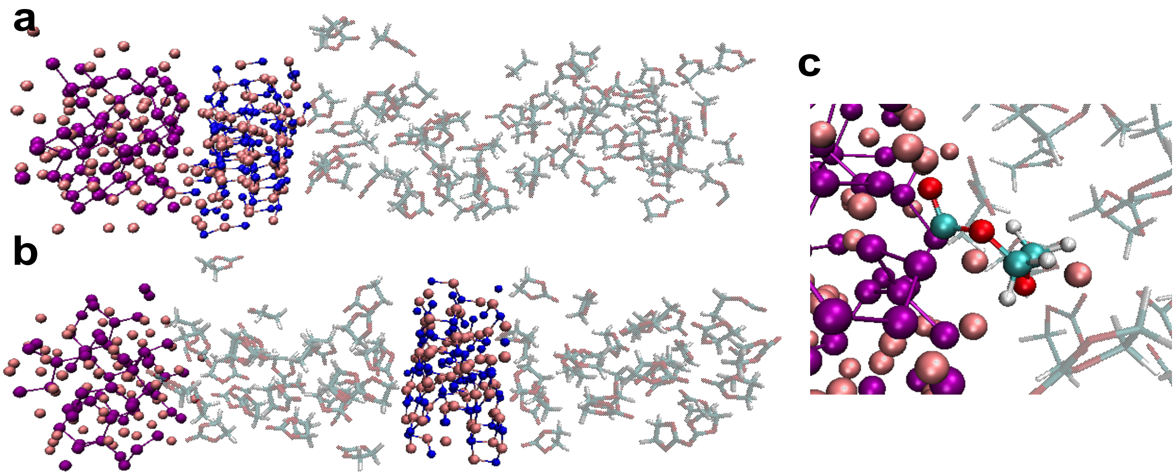

Figure S11. DFT-MD snapshots of lithiated silicon electrode / EC electrolyte interface with LiF aggregate. The electrode and LiF aggregate are shown in the ball and stick style, while the diaphanous tube style is used for EC solvent molecules. Cyan, white, red, blue, purple, and pink colors denote C, H, O, F, Si and Li atoms, respectively. (a) Adsorbed structure of LiF aggregate adsorbed to graphite anode. (b) Dissolved structure of LiF aggregate in EC electrolyte. (c) Decomposed EC molecule near lithiated silicon electrolyte.

On the other hand, we can clearly see the binding structure between lithiated silicon anode and LiF aggregate by comparing the DFT-MD snapshots of t=0 (initial state of DFT-MD) and t=10ps (sufficiently equilibrium state) at the interface of the lithiated silicon anode and the LiF aggregate. We show the t=0 and t=10 ps DFT-MD snapshots in Fig.S12. It is likely that this binding of Li-F stables the adsorption of LiF aggregate to silicon anode.

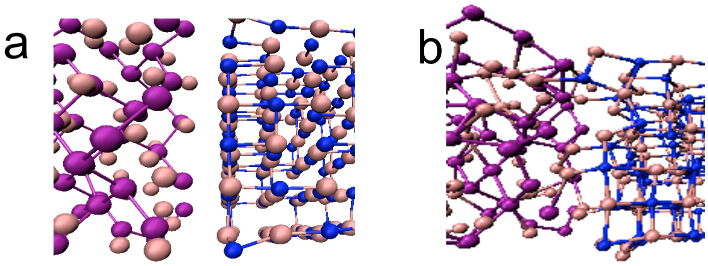

Figure S12 DFT-MD snapshots of the interface structure of lithated silicon/LiF aggregate/ EC solvent system. Blue, purple, and pink colors denote F, Si and Li atoms, respectively. (a) and (b) show t=0 (initial state) and t=10 (equilibrium state) ps DFT-MD snapshots, respectively.